J Appl Electrochem (2008) 38:497–505
DOI 10.1007/s10800-007-9463-5

ORIGINAL PAPER

Current and voltage distributions in a tubular solid oxide fuel cell (SOFC)

J.-M. Klein · Y. Bultel · M. Pons · P. Ozil

Received: 26 April 2007 / Revised: 28 November 2007 / Accepted: 28 November 2007 / Published online: 11 December 2007
© Springer Science+Business Media B.V. 2007

Abstract One of the major obstacles to improving electrochemical performance of SOFCs is the limitation with respect to current collecting. The aim of this study is to examine these limitations on the basis of a model of a single cell of tubular SOFC. The simulation results allow us to understand and analyze the effects of ionic and electronic ohmic drops on cell performance. This paper describes a model using the CFD-Ace software package to simulate the behaviour of a tubular SOFC. Modelling is based on solving conservation equations of mass, momentum, energy, species and electric current by using a finite volume approach on 3D grids of arbitrary topology. The electrochemistry in the porous gas diffusion electrode is described using Butler-Volmer equations at the triple phase boundary. The electrode overpotential is computed at each spatial location within the catalyst layer by separately solving the electronic and ionic electric potential equations. The 3D presentation of the current densities and the electronic and ionic potentials allows analysis of the respective ohmic drops. The simulation results show that the principal limitations are at the cathodic side. The limitations due to ionic ohmic drops, classically considered to be the main restrictions, are confirmed. The particular interest of our study is that it also shows that, because of the cylindrical geometry, there is a significant electronic ohmic drop.

J.-M.Klein (✉) · Y. Bultel · P. Ozil
Laboratoire d'Electrochimie et de Physico-Chimie des Matériaux et des Interfaces (LEPMI), UMR 5631 CNRS-INPG-UJF, ENSEEG, BP 75, 38402 Saint Martin d'Heres, France
e-mail: jean-marie.klein@lepmi.inpg.fr

M. Pons
Laboratoire de Thermodynamique et de Physicochimie Métallurgique (LTPCM), UMR 5614 CNRS-INPG-UJF, ENSEEG, BP 75, 38402 Saint Martin d'Heres, France

Keywords Tubular SOFC · Modelling · Simulation · Voltage/Current distribution

Nomenclature

D_i	Diffusion coefficient of the ith species ($m^2\ s^{-1}$)
D_{ieff}	Effective diffusion coefficient of the ith species ($m^2\ s^{-1}$)
E_0	Voltage between the electrolyte and the nickel at equilibrium (V)
F	Faraday constant (96,500) (C mol^{-1})
J_i	Diffusion flux of the i-th species (kg $m^{-2}\ s^{-1}$)
M	Molecular weight of the mixture of gases (kg $kmol^{-1}$)
P_i	Partial pressure of the ith species (Pa)
R	Universal gas constant (8,314) (J $mol^{-1}\ K^{-1}$)
$(S/V)_{eff}$	Effective surface-to-volume ratio ($m^2\ m^{-3}$)
T	Temperature (K)
d_{pore}	Pore diameter (m)
h	Gas mixture enthalpy (J kg^{-1})
h_i	Enthalpy of the ith species (J kg^{-1})
h_B	Solid phase enthalpy (J kg^{-1})
$[i]$	Molar concentration of the ith species (kmol m^{-3})
$[i]_0$	Reference concentration of the ith species (kmol m^{-3})
j_{a0}	Exchange current density of the anode (A m^{-2})
j_{at}	Faradaic current due to anodic reaction (A m^{-2})
p	Total pressure (Pa)
q	Heat flux (W m^{-2})
v	Fluid velocity (m s^{-1})
w_i	Mass fraction of the ith species

Greek

α_a	Anodic Tafel constant
α_c	Cathodic Tafel constant

ε	Porosity
ϕ_S	Ionic phase potential at anode (V)
ϕ_M	Electronic phase potential at anode (V)
λ	Thermal conductivity of the porous medium (W m^{-1} K^{-1})
η_a	Anode overpotential (V)
κ	Permeability (m^2)
μ	Dynamic viscosity of the gas mixture (Pa s)
v_i'', v_i'	Normalized stoichiometric coefficients
ρ	Mass density of the gas mixture (kg m^{-3})
ρ_B	Mass density of the solid phase (kg m^{-3})
σ_S	Ionic phase conductivity at anode (Ω^{-1} m^{-1})
σ_M	Electronic phase conductivity at anode (Ω^{-1} m^{-1})
τ	Tortuosity of pores (m m^{-1})

1 Introduction

SOFCs (Solid Oxide Fuel Cells) are promising candidates for generating power while preserving the environment. Since all SOFC components are solid state, in principle there are no restrictions on cell configuration. The cell can be shaped according to criteria that enable design or application problems to be overcome. Cells are being developed in two different configurations: tubular and planar. A major advantage of the tubular design is that high temperature gas-tight seals are eliminated. In tubular SOFCs, individual fuel cells are built up in layers on the support tube and are connected in series by a ceramic interconnect material to form a stack. Because the current flows along a relatively long path around the circumference of the cell to the interconnect, significant ohmic losses can occur.

Recent literature provides evidence of significant research and development efforts focused on modelling within the SOFC anode. Lehnert et al. [1] proposed one-dimensional simulations based on a geometry integrating an anode supported by a planar substrate and taking into account mass transport. Multi-component transport was described using the Mean Transport Pore Model (MTPM), based on three microstructure parameters (porosity, tortuosity and mean pore radii). Suwanwarangkul et al. [2] focused on concentration polarization in different models (Fick's law, dusty-gas and Stefan-Maxwell models) for a $H_2/H_2O/CO/CO_2$ mixture. The MTPM model was extended by Ackmann et al. [3] into a two-dimensional thermal approach including electrochemical and chemical reactions as heat sources. Some more recent studies describe models of SOFCs based on detailed electrochemical analyses and fluid-dynamic calculations of internal heat transfer conditions using a finite volume method [4–6]. Finally, some general models have been developed, taking into account velocity fields of air and fuel flows, heat generation by ohmic and thermodynamic effects and convective heat-transfer, while other studies have focused on the mass transfer of active chemical species, including electrochemical processes and the distribution of electric potential within electrodes and electrolyte [7, 8]. In most of these approaches, the charge balance equation is solved by considering whether the cell potential and the current density along the SOFC length are constant.

A number of studies have already been carried out on the current collecting aspects of electrochemical cells. Matlosz et al. [9] studied the secondary current distribution in a Hull cell. The study of these limitations from a generator point of view is nowadays, less advanced. Fontes et al. [10] showed that for MCFC cathodes with a finite electronic conductivity there is a substantial potential distribution perpendicular to the depth of the electrode. In the SOFC, Schneider et al. [11] studied the influence of percolation on electronic conductor performance.

The aim of the present study is to assess the influence of geometry and ionic and electronic conductivities on SOFC steady state performance. A model of a tubular SOFC was developed using the CFD software package developed by CFD RC. A realistic triple phase boundary distribution is considered through the porous electrode thickness. The electrochemical reactions within the porous electrodes are described using the Butler–Volmer equations at the triple phase boundary. Modelling is based on solving the conservation equations of mass, momentum, energy, species and electric current by using a finite volume approach on 3D grids of arbitrary topology. Simulations with the CFD software package allow the calculation of the distributions of partial pressures, current density and potentials of electronic and ionic phases within the anode part (i.e. gas channel and electrodes). In actual SOFC operation, since the current is collected by the interconnect, the current magnitude through each electrode changes in the peripheral direction. There are peripheral ionic and electronic current nonuniformities, which in turn causes nonuniformity of mass transfer and heat generation. So in this paper, the authors are able to use CFD software to solve this computationally expensive 3D problem.

The study is applied to a relatively old SOFC configuration, which is not state-of-the-art. Tubular cell performance limitations due to the long current flow path along the circumferential direction are a well known issue, and the major tubular SOFC manufacturers have already abandoned this cell design in favour of flat tube and more developed designs. Detailed information regarding these designs is difficult to be found in the open literature.

However the goal of this paper is to present a methodology to analyse the effects of ohmic losses and particularly the influence of electronic ohmic drops on the performance of the cell with a CFD software package. Finally the methodology presented here can also be applied to more recent cell designs.

2 Tubular SOFC model

2.1 Description of the tubular SOFC

A Tubular SOFC is a cylindrical assembly comprising an electrolyte sandwiched between an anode and a cathode. The design of the cell is conceived on the basis of the classical unit cell developed by Siemens Westinghouse. The oxidant gas is introduced through a central injection tube, and the fuel gas is supplied to the exterior of the tube. The fuel gas flows past the anode on the exterior of the cell parallel to the oxidant gas (co-flow). The tube length for modelling purposes is 5 mm and the radii of the different parts of the SOFC are given in Table 1. These may be different from the real Westinghouse ones due to the lack of better information.

This model is based on a cathode-supported geometry as shown in Fig. 1 to which was added a central support tube in alumina to improve the mechanical resistance of a stacking. The characteristic components of the tubular SOFC are also identified.

Rectangular meshes are used to grid this geometry [12].

In the present model, mass and charge transport phenomena coupled with chemical and electrochemical reactions are investigated within the inlet of a tubular SOFC as shown in Fig. 1. A finite volume method using a computational grid [13, 14] is used to solve mass, charge, energy, momentum balances including transport through porous media, and chemical and electrochemical reactions within the porous electrodes in a gas diffusion electrode model. In this model, steady state conditions are imposed.

Table 1 Geometric parameters of the tubular SOFC

Geometry	Inner radius (mm)	Outer radius (mm)
Tube support	5.00	6.50
Cathode	6.50	7.20
Electrolyte	7.20	7.26
Interconnection	7.20	7.26
Anode	7.26	7.36
Fuel channel	–	10

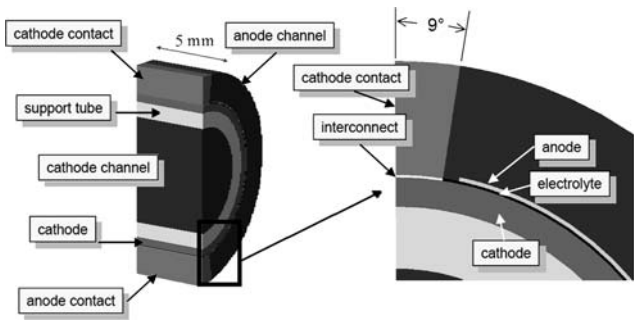

Fig. 1 Geometry of the tubular SOFC cell

The O_2/N_2 (0.21 wt%, 0.73 wt%) and $H_2/H_2O/CO/CO_2$ (0.096 wt%, 0.428 wt%, 0.26 wt%, 0.216 wt%) mixtures are respectively supplied at the air cathode with a mass flow rate of 3.415×10^{-6} kg s^{-1} and the anode gas channel with a mass flow rate of 2.12×10^{-5} kg s^{-1}. The cell inlet temperature is set to 1,173 K.

In the gas phase, mass conservation is described as follows [13]:

$$\frac{\partial}{\partial t}(\varepsilon\rho) + \nabla \cdot (\varepsilon\rho\mathbf{v}) = 0 \tag{1}$$

where ε is the porosity of the medium, ρ is the density and $\mathbf{v}$ is the velocity vector of the gas mixture.

By ignoring compressibility and turbulence effects, the conservation equations for the transport of Nth species in a porous medium can be presented in the following vector form:

$$\frac{\partial}{\partial t}(\varepsilon\rho\mathbf{v}) + \nabla \cdot (\varepsilon\rho\mathbf{v} \cdot \mathbf{v}) = -\varepsilon\nabla p + \nabla \cdot (\varepsilon\boldsymbol{\delta}) + \frac{\varepsilon^2\mu\mathbf{v}}{\kappa} \tag{2}$$

where p is the pressure, $\boldsymbol{\delta}$ the shear stress tensor, μ the dynamic viscosity of the fluid. κ is the permeability and represents the square of the effective volume-to-surface area ratio of the porous matrix. The last term in Eq. 2 represents Darcy's drag force imposed by the pore walls on the fluid and usually results in a significant pressure drop across the porous medium.

The conservation equation for energy (Eq. 3) may be written as [14, 15]:

$$\frac{\partial}{\partial t}[(1-\varepsilon)\rho_B h_B + \varepsilon\rho h] + \nabla \cdot (\varepsilon\rho\mathbf{v}h) = \nabla \cdot \mathbf{q} + \varepsilon\boldsymbol{\delta} \cdot \nabla\mathbf{v} + \varepsilon\frac{\mathrm{d}p}{\mathrm{d}t} - j_t\left(\frac{S}{V}\right)_{\mathrm{eff}}\eta + \frac{|\mathbf{i}\cdot\mathbf{i}|}{\sigma} \tag{3}$$

where h is the gas mixture enthalpy. h_B and ρ_B are, respectively, the solid phase enthalpy and density. The heat flux, $\mathbf{q}$, is comprised of contributions due to thermal conduction and species diffusion (Eq. 4), and is written as:

$$\mathbf{q} = \lambda\nabla T + \sum_i \mathbf{J}_i h_i \tag{4}$$

h_i being species i enthalpies (defined here as sum of the enthalpy of formation and the sensitive enthalpy), $\mathbf{J}_i$ their diffusion fluxes, and T the temperature. The thermal conductivity, λ, of the porous medium is an effective thermal conductivity of the fluid and solid regions taken together [13]. The last two terms in Eq. 3 represent electrical work and Joule heating, respectively. The irreversible losses due to the reaction (conversion of chemical energy to heat energy) manifest themselves automatically through the second term on the right hand side of Eq. 4 because the definition of enthalpy includes both the enthalpy of formation and the sensible enthalpy.

The cell walls are considered adiabatic. The conservation equation for energy (Eq. 3) is solved in each volume element and a continuity condition is imposed at interfaces. Then the specific heat transfer coefficients are calculated by the classical Jannaf method. Knowing the enthalpy and the heat transfer coefficients it is thus possible to assess the temperature distributions. However the heat transfer by radiation is not taken into account here because of the weakness of the temperature gradient in the cell.

Mass and charge balances are numerically solved with regard to the following boundary conditions. Potentials are set to zero for the anodic collector and to an input value for the cathodic one. First the cathodic potential is set to 0.6 V. Then this potential is varied in order to obtain the polarization curves. Ionic current is assumed to be zero on the surface of both collectors but variable elsewhere. Electronic ohmic drops along the gas channel can be ignored because of the high electronic conductivity assumed for the electronic conductor. This hypothesis is confirmed by the work of Bultel et al. [16].

Finally, gas transport within the porous electrode is described by using the combination of diffusive transport (Stefan-Maxwell and Knudsen diffusions) and convective transport.

2.2 Electrodes

The anode material is a nickel and yttrium stabilized zirconia cermet (Ni–YSZ). The anode is considered for modelling purposes as a porous gas diffusion electrode wherein the electrochemical reaction occurs at the triple phase boundary, i.e. at the interface between the electronic and ionic conductor, and gas phase. Current density is thus the sum of two quite distinct contributions: one related to ionic species and the other to electron transport. Mass transport occurs within the gas pores and charge transport phenomena depend on four electric parameters: ionic and electronic conductivities σ_{as}, σ_{aM} (Ω^{-1} m^{-1}) and potentials ϕ_{aS} and ϕ_{aM} (V).

The cathode is a porous lanthanum manganite ($La_{0.7}Sr_{0.3}MnO_{3-\delta}$) doped with YSZ solid phases. Its behaviour is described in the same way as previously for the anode.

Hydrogen is electrochemically oxidized within the anode (Eq. 5) while oxygen is electrochemically reduced (Eq. 6):

$$H_2 + O^{2^-} \rightarrow H_2O + 2e^- \quad (5)$$

$$1/2O_2 + 2e^- \rightarrow O^{2^-} \quad (6)$$

The kinetics of the electrochemical reactions (Eqs. 5 and 6) within the porous electrode can be described using the Butler–Volmer equation at the triple phase boundary. It can be written like Eq. 7 for the anode reaction:

$$j_{at} = j_{a0}\left(\exp\left(\frac{\alpha_a F}{RT}\eta_a\right)\frac{[H_2]}{[H_2]_0} - \exp\left(-\frac{\alpha_c F}{RT}\eta_a\right)\frac{[H_2O]}{[H_2O]_0}\right) \quad (7)$$

Here the faradaic current density is expressed in A m^{-2}. The overpotential η (Eq. 8) is defined as the difference between electronic (ϕ_{aM}) and ionic (ϕ_{aS}) potential as:

$$\eta_a = \phi_{aM} - \phi_{aS} - E_{a0} \quad (8)$$

and is locally determined within the porous electrode by separately solving the equations related to electronic and ionic potentials. E_{a0} is the potential difference between the electrolyte and the nickel at equilibrium, i.e., when no current is flowing.

The other parameters are the symmetry factors α_a and α_c determined from the experimental Tafel slopes, the exchange current density j_{a0} (A m^{-2}), the Faraday constant F and the ideal gas law constant R. $[i]$ is the interfacial concentration while $[i]_0$ refers to concentration values at the reference state at which the reference current density is prescribed.

The kinetic data used in the Butler–Volmer equations (exchange current density j_0 [17], symmetry factors α_a and α_c) are summarized in Table 2 for both anode and cathode.

The current in a porous electrode can be split into two parts: one part flowing through the electrolyte phase and the other through the electronic phase of the porous matrix. During electrochemical reactions, electrons are then transferred from the ionic phase to the electronic phase, or vice versa. If we consider an electrochemical reaction, charge conservation may thus be expressed from Ohm's law (Eq. 9) as:

$$\nabla\cdot(\sigma_S\nabla\Phi_S) = -\nabla\cdot(\sigma_M\nabla\Phi_M) = j_t\left(\frac{S}{V}\right)_{eff} \quad (9)$$

Mass balances for each gas phase species i are given at steady state by Eq. 10:

$$\nabla\cdot(\varepsilon\rho\mathbf{v}w_i) = \nabla\cdot\mathbf{J}_i + M_i\left(\nu_i'' - \nu_i'\right)\left(\frac{S}{V}\right)_{eff}\frac{j_t}{F} \quad (10)$$

The left side is the convective term. On the right side, J_i is the diffusion flux and the last term is the source term for the creation or consumption rate of species i (per unit

Table 2 Kinetic data for electrochemical reactions

	Anode	Cathode
$(S/V)\ j_0$/A m^{-3}	10^{12}	10^{10}
α_a	0.7	–
α_c	–	0.7

volume of porous medium) resulting from the electrochemical reactions (Eqs. 5 and 6). v_i' and v_i'' are respectively the normalized stoichiometric coefficients for reactants and products, M_i is the molecular weight of species i, $(S/V)_{\text{eff}}$ ($\text{m}^2\ \text{m}^{-3}$) is used to take into account the effective surface-to-volume ratio which is directly linked to the triple phase boundary surface area per unit electrode volume. For the description of the diffusion term found in Eq. 10, the diffusion flux is given by:

$$\mathbf{J}_i = \rho D_{i,\text{eff}} \nabla w_i + \frac{\rho w_i}{M} D_{i,\text{eff}} \nabla M + \rho w_i \sum_j D_{j,\text{eff}} \nabla w_j + \rho w_i \frac{\nabla M}{M} \sum_j D_{j,\text{eff}} w_j \quad (11)$$

depending on the mass fraction of species i, the mass fraction j of all the other components of the mixture and the molar mass of the gas mixture.

The effective mass diffusion coefficient $D_{i,\text{eff}}$ is used to take into account the porous medium in the Stefan-Maxwell diffusion (Eq. 11) relation [18], and is to be deduced from the free stream diffusion coefficient D_i by the so-called Bruggemann model [19] depending on tortuosity τ. Simulations were performed here with a tortuosity of 1.5, a classical value from the literature [20, 21] in the absence of more accurate data.

2.3 Electrolyte

The electrolyte material is YSZ, which is a suitable ionic conductor at high temperatures. Conditions of zero electronic current and zero electronic voltage are imposed in the electrolyte to ensure that the electrolyte is completely impermeable to electron circulation. The electrolyte potential is thus expressed by a classical Ohm's law (Eq. 9) without any charge creation or consumption within the electrolyte.

2.4 Simulation parameters

Table 3 provides a brief description of the properties [22–26] of the materials currently used in the various cell components at 1,173 K. The major heat sources in SOFCs are produced by chemical and electrochemical reactions. The low cell length taken into account in this study (5 mm) limits strongly the temperature increase in the cell. The material parameters can thus be assumed constant. This is confirmed by the results with only a 4 K temperature gradient in the cell.

Finally the description is completed by the ideal gas law.

3 Results

Gas phase diffusion and ionic migration limitations are generally considered at the electrode when examining current collecting contribution [11]. Nevertheless, electronic ohmic drop may be significant in the cell, depending on the geometry and operating conditions. The effect of current and voltage distributions within a tubular SOFC are investigated on the basis of the previously described 3D model. We observe a drop in cell voltage or power density, which cannot reach its maximum value. The study therefore aims to analyze problems related to the cell geometry.

Because the current flows in the circumferential direction of the cell, a relatively small cell length can be considered for simulation. Current collecting limitations are thus only of a radial or orthoradial nature and not longitudinal. Since SOFC performance is controlled by the oxygen reduction reaction, this study focuses mainly on the effect of the cathode support. In fact, since the electrochemical hydrogen reduction reaction is very fast compared with the cathodic one ($j_{a0} = 100\ j_{c0}$, cf. Table 2), the anode overpotential is assumed negligible. Moreover due to the low thickness of the anode, the ionic ohmic losses at the anode side can also be neglected. Nevertheless, the electronic ohmic drop could be significant.

Since oxide ions migrate from the cathode towards the anode through the electrolyte, the ionic current density is uniformly distributed along the circumference of the cell and is mainly radial.

The ionic potential distribution enables us to assess the ionic ohmic drop within the cathode. Since a thick cathode is used, the ohmic drop limitation is quite considerable. It is worth mentioning that a very steep gradient is observed closed to the electrode/electrolyte interface. Nevertheless, the equipotential curvature (orthogonal to the ionic current densities) shows that the effect of the ionic ohmic drop limitation on cell performance is independent of the cell configuration (tubular or planar SOFC). The ionic potential

Table 3 Material properties at 1,173 K

Material	$\sigma_S/\Omega^{-1}\ \text{m}^{-1}$	ε	κ/m^2	$\lambda_B/\text{W m}^{-1}\ \text{K}^{-1}$	d_{pore}/m	$\sigma_M/\Omega^{-1}\ \text{m}^{-1}$
Anode Ni–YSZ	3.5	0.50	1×10^{-12}	6.23	1×10^{-6}	5×10^4
Cathode LaMnO3–YSZ	1.8	0.40	1×10^{-12}	9.6	1×10^{-6}	7.7×10^3
Electrolyte YSZ	7	0.001	1×10^{-18}	2.7	1×10^{-6}	–

change from the gas channel/cathode interface to the cathode/electrolyte interface is about 160 mV. This phenomenon is due to the ionic conductivity (σ_S) of the material, which is not high enough when the SOFC temperature is decreased or the cathode thickness is increased.

Figure 2a and b presents the electronic current density at the cathode and the electronic potential distribution at the cathode and the anode side. Unlike the ionic phase behaviour, both the electronic current density and the potential vary considerably around the cell circumference between the cathode collector and the opposite side because the electronic conductivity of the LSM–YSZ composite (Lanthanum Manganite–YSZ) is not high enough. There is thus an orthoradial change in the electronic ohmic potential of about 170 mV from the cathode collector to the opposite side (i.e. over the anode collector). Nevertheless, it clearly appears that, for a tubular SOFC, from a radial point of view, the electronic ohmic drop is negligible (Fig. 2b). It can thus be stated that the electronic phase is constant along the cell radius. Although the electronic conductivity of the anode is relatively significant, the anodic behaviour is similar to that of the cathodic. Indeed the value of the electronic ohmic drop in the anode is nearly the same as that in the cathode. This result is very intriguing. However an explanation to this phenomenon can be proposed. The current collecting being done between the anodic and cathodic collectors, the value of the cell potential must be independent of the route followed. This is why the electronic ohmic drop in the anode seems to be governed by the electronic ohmic drop in the cathode where the electronic conductivity is limiting.

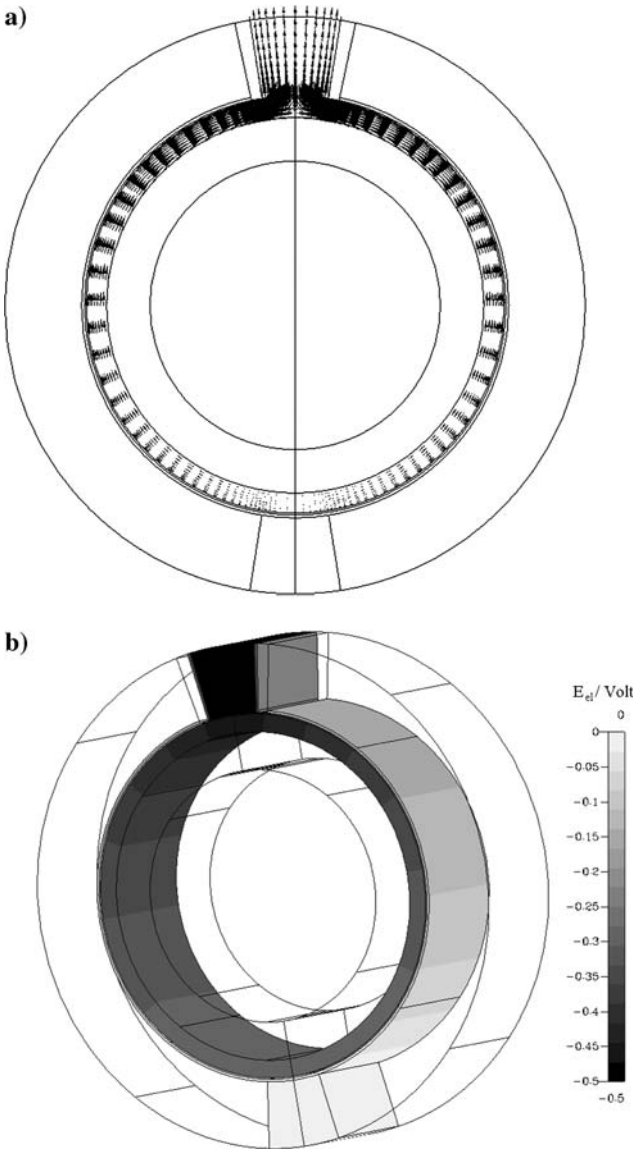

Fig. 2 (**a**) Electronic current density in the cathode (**b**) Electronic phase potential at the cathodic and anodic side

4 Discussion

Having established the influence of both ionic and electronic current collecting, we shall now look at their effect on the tubular SOFC performance.

4.1 Overpotential at the cathode

The overpotential distribution resulting from the electronic and ionic potential distributions (see Eq. 8) is presented on Fig. 3a.

Although there is a significant change in both ionic and electronic potential through the composite cathode, the overpotential distribution is uniform along the circumference of the cell, similar to the ionic potential distribution. It should be remembered that the electronic phase exhibits equipotential behaviour around the cell radius (see Fig. 2 b). Since it is essentially the electrochemical reaction and the ionic transport that control the process kinetics, an increase in the absolute value of the overpotential can be observed along the cell radius from the gas/cathode interface (Fig. 3b) to reach a maximum value of about 170 mV. This theoretical result is in agreement with the classical continuum model for a composite cathode [27]. At the anode side, overpotential is very weak owing to the fast electrochemical hydrogen oxidation reaction. Nevertheless, similar electrical distributions are predicted.

Even though diffusion limitation is generally assumed to be negligible with regard to ionic ohmic drop for an SOFC composite cathode [27], Fig. 4 shows that the oxygen partial pressure distribution through the composite cathode is not constant. As expected, very low oxygen depletion through the cathode thickness can be observed depending on the coordinates. Further concentration overpotential

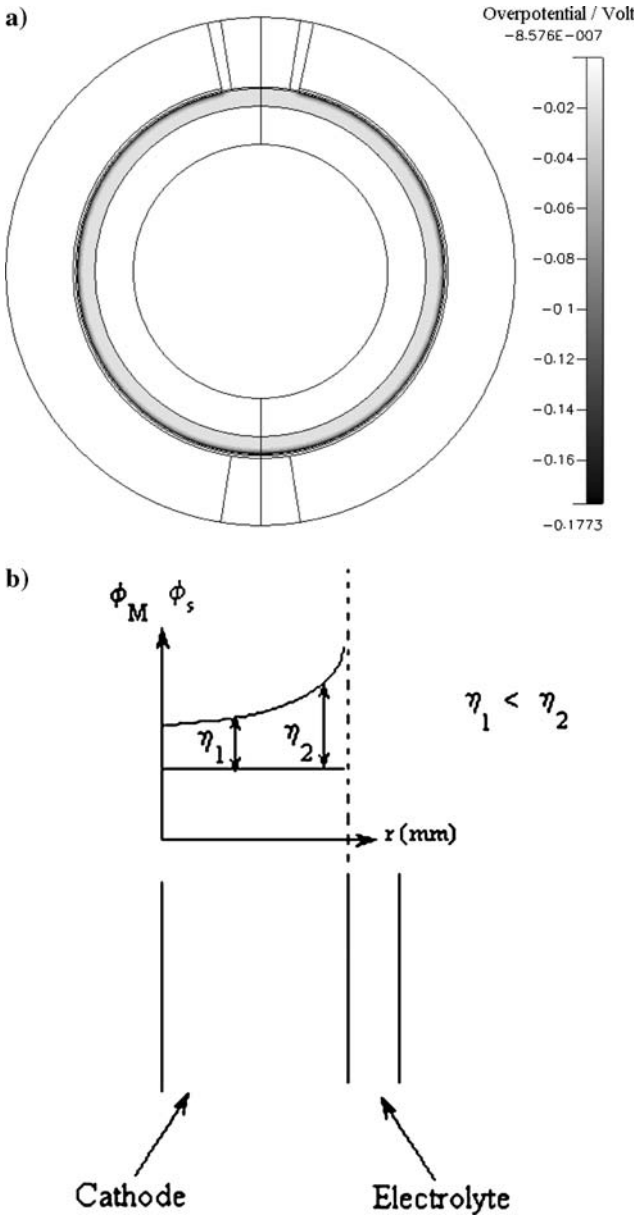

Fig. 3 (**a**) Overpotential distribution at the cathode (**b**) Influence of cell radius on overpotential

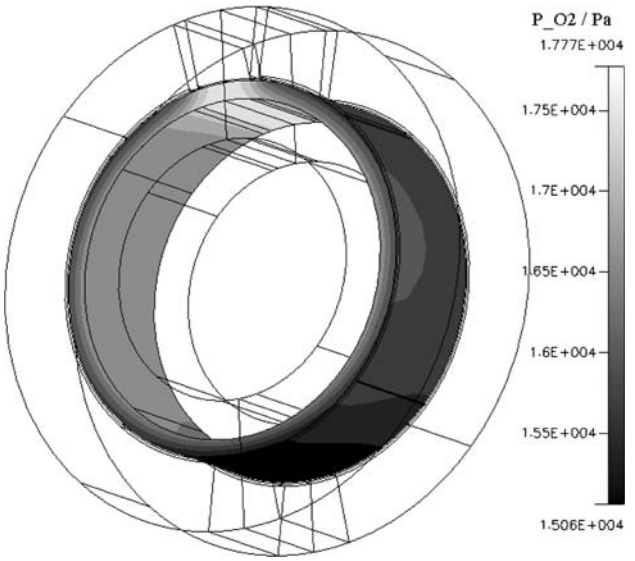

Fig. 4 Oxygen partial pressure

induced by diffusion limitation can thus be ignored for this working point (0.43 A cm^{-2}). Nevertheless, it should be noted that the cathode part located under the cathodic collector is electrochemically inactive due to the cell configuration and the distance of this area from the electrolyte, while the largest concentration depletions are observed close to the anodic collector.

4.2 Reaction localisation

In order to fully investigate the influence of the tubular SOFC cell geometry on performance, Fig. 5a presents the faradaic current density distribution at the cathode. The faradaic current density is uniformly distributed and increases radially from the gas/cathode interface to the cathode/electrolyte interface, in exactly the same way as the cathodic overpotential.

A composite electrode is made up of a porous mixture of electrocatalyst and ionic particles, so it theoretically increases the electrode performance by spreading the reaction zone from the electrode/electrolyte interface into the entire thickness of the electrode. Because of the poor ionic ohmic conductivity, the majority of the reaction is nevertheless localised close to the electrolyte. Indeed the faradaic current gradient is the strongest in this area.

The zooms in Fig. 5b and c show parts of the cathode close to the cathodic and anodic collectors. In Fig. 5b, the electrochemical reaction is even more favoured due to the low electronic ohmic drop contributions. In Fig. 5c, the electrochemical reaction is also favoured, in this case due to the proximity of the anodic collector. Finally, under the cathode collector, the faradaic current is zero due the large ionic ohmic drop contribution. A relationship can be observed between these results and those in Fig. 4, which present the oxygen partial pressure at the cathode. Thus, the lowest oxygen partial pressures are found close to the current collectors.

4.3 Polarization curves

Figure 6 presents the simulated polarization curves for our tubular SOFC geometry. A sensitivity analysis is performed by increasing the electronic conductivity from the standard case ($\sigma_M = 7{,}700$ S m^{-1}) to a high value

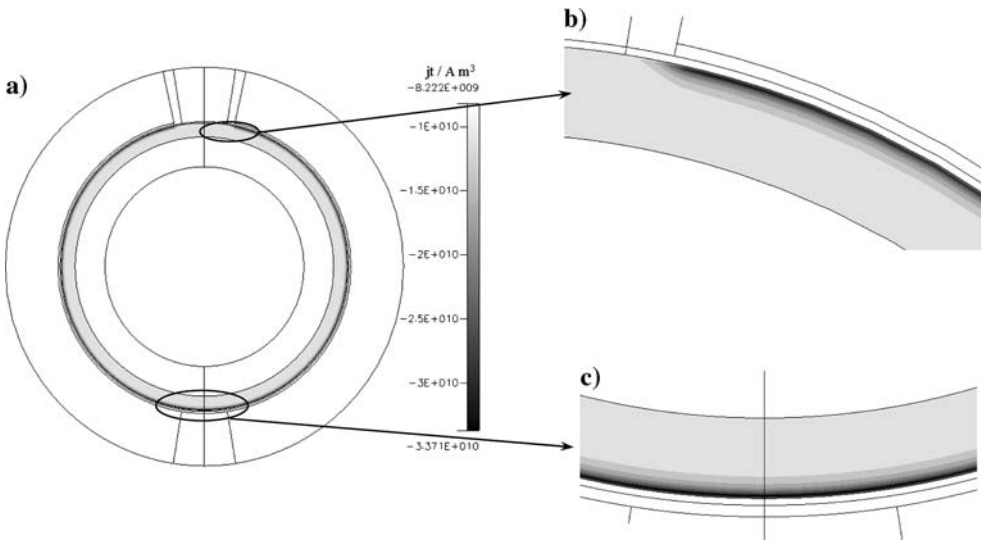

Fig. 5 (**a**) Faradaic current density at the cathode (**b**) Zoom presenting part of the cathode close to the cathodic collector (**c**) Zoom of the cathode over the anodic collector

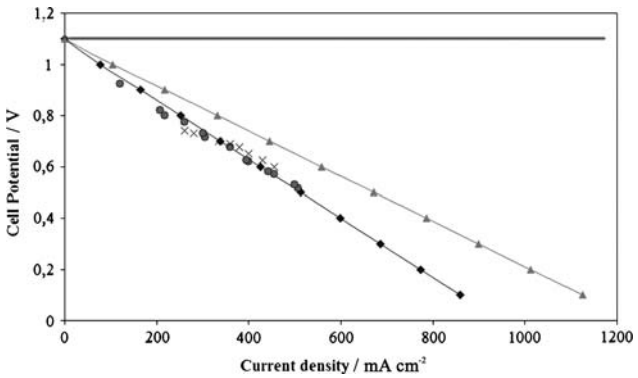

Fig. 6 Simulated polarization curves. ◆, Simulated polarization curve for $\sigma_M = 7{,}700$ S m^{-1}; ▲, Simulated polarization curve for $\sigma_M = 5 \times 10^4$ S m^{-1}; ●, Model data [12] × Experimental data [34]

($\sigma_M = 5 \times 10^4$ S m^{-1}). For the standard case, a current density of 425.4 mA cm^{-2} is reached for a cell potential of 0.6 V, corresponding to a 0.5 V loss, compared with the ideal situation (1.1 V). This drop is the sum of the ionic ohmic drop, the electronic ohmic drop and the overpotential contributions. In the case of a very high electronic conductivity it may be noted that for the same current density the performance of the cell is higher, being close to 0.7 V. Indeed, the electronic ohmic drops are less significant because of the higher electronic contribution.

Some experimental and model data have been added to the polarization curve [8, 28]. However geometries used in these works are not exactly the same as that used in our study. Nevertheless, quite good agreement between experimental and simulated (Fig. 6) polarization curves is obtained. Hagiwara et al. [29] have also proposed some experimental data which have the same order of magnitude.

5 Conclusion

A model using the CFD-Ace software package has been developed for studying the collecting effects at the cathode side of a cathode-supported tubular SOFC. Through the simulations, current density and the potentials of the electronic and ionic phases within the cathode side were predicted. The limitations due to ionic ohmic drop, classically considered to be the principal restrictions, were also confirmed.

In addition, we have shown that the geometry of the cell can influence performance because of the non-uniform orthoradial distribution of the electronic contribution. Our simulations show that for a low electronic conductivity there is a strong potential gradient around the circumference of the cell. This potential gradient indicates the existence of a considerable electronic ohmic drop in this tubular cell.

Acknowledgment The authors extend their warmest thanks to Dr J. Deseure for many fruitful discussions.

References

1. Lehnert W, Meusinger J, Thom F (2000) J Power Sources 87:57
2. Suwanwarangkul R, Croiset E, Fowler MW, Douglas PL, Entchev E, Douglas MA (2003) J Power Sources 122:9
3. Ackmann T, de Haart LGJ, Lehnert W, Stolten D (2003) J Electrochem Soc 150(6):A783
4. Morel B, Laurencin J, Bultel Y, Lefebvre-Joud F (2005) J Electrochem Soc 152(7):A1382
5. Larrain D, Van Herle J, Maréchal F, Favrat D (2003) J Power Sources 118:367
6. Campanari S, Iora P (2004) J Power Sources 132:113
7. Aguiar P, Adjiman CS, Brandon NP (2004) J Power Sources 138:120
8. Li PW, Suzuki K (2004) J Electrochem Soc 151(4):A548

9. Matlosz M, Creton C, Clerc C, Landolt D (1997) J Electrochem Soc 134(12):3015
10. Fontes E, Fontes M, Simonsson D (1996) Electrochim Acta 41:1
11. Schneider LCR, Martin CL, Bultel Y, Bouvard D, Siebert E (2006) Electrochim Acta 52:314
12. CFD Research Corporation (2003) Tutorial Short-SOFC
13. Klein J-M, Bultel Y, Georges S, Pons M (2007) Chem Eng Sci 62:1636
14. Mazumder S, Cole JV (2003) J Electrochem Soc 150(1):A1503
15. Wang CY, Cheng P (1997) Adv Heat Transf 30:93
16. Bultel Y, Gautier L, Zahid M, Stevens P, Klein J-M (2007) J Electrochem Soc Trans 7(1):1791
17. Costamagna P, Panizza M, Cerisola G, Barbucci A (2002) Electrochim Acta 47:1079
18. Bird RB, Byron R, Stewart WE, Lightfoot EN (1960) In: John Wiley & Sons (ed) Transport phenomena, New York
19. Bruggemann DAG (1935) Ann Physik 24:636
20. Springer TE, Zawodinski TA, Gottesfeld S (1991) J Electrochem Soc 138(8):2334
21. Natarajan D, Nguyen TV (2001) J Electrochem Soc 148(12):A1324
22. EG&G Services (2000) In: Science applications international corporation (ed) Fuel cell handbook, 5th edn, pp 8–5
23. Aruna ST, Muthuraman M, Patil KC (1998) Solid State Ionics 111:45
24. Hecht ES, Gupta GK, Zhu H, Dean AM, Kee RJ, Maier L, Deutschmann O (2005) Appl Catal 295:40
25. Lee JH, Moon H, Lee HW, Kim J, Kim JD, Yoon KH (2002) Solid State Ionics 148:15
26. Ullmann H, Trofimenko N, Tietz F, Stöver D, Ahmad-Khanlou A (2000) Solid State Ionics 138:79
27. Deseure J, Bultel Y, Dessemond L, Siebert E (2005) Electrochim Acta 50:2037
28. Incropera FP, DeWitt DP (1996) In: John Wiley & Sons (ed) Introduction to heat transfer, 3rd edn, New York
29. Hagiwara A, Michibata H, Kimura A, Jaszcar MP, Tomlins GW, Veyo SE (1999) Proceedings of the third international fuel cell conference, D2-4, p 369